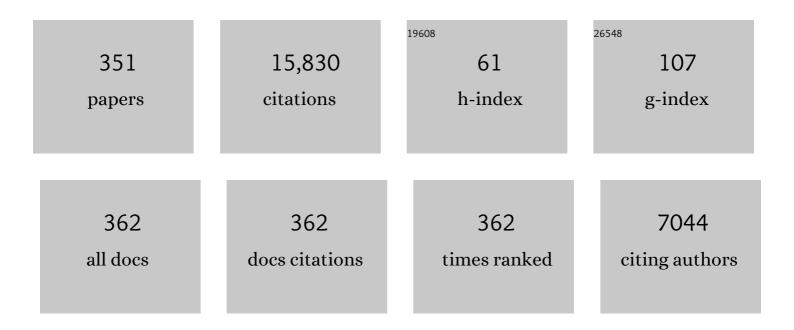
Daolun Chen

List of Publications by Year in descending order

Source: https://exaly.com/author-pdf/8818241/publications.pdf Version: 2024-02-01



#	Article	IF	CITATIONS
1	Consideration of Orowan strengthening effect in particulate-reinforced metal matrix nanocomposites: A model for predicting their yield strength. Scripta Materialia, 2006, 54, 1321-1326.	2.6	1,098
2	Latest research advances on magnesium and magnesium alloys worldwide. Journal of Magnesium and Alloys, 2020, 8, 1-41.	5.5	852
3	Contribution of Orowan strengthening effect in particulate-reinforced metal matrix nanocomposites. Materials Science & Engineering A: Structural Materials: Properties, Microstructure and Processing, 2008, 483-484, 148-152.	2.6	592
4	Research advances in magnesium and magnesium alloys worldwide in 2020. Journal of Magnesium and Alloys, 2021, 9, 705-747.	5.5	499
5	Strain hardening behavior of a friction stir welded magnesium alloy. Scripta Materialia, 2007, 57, 1004-1007.	2.6	351
6	Microstructure and tensile properties of friction stir welded AZ31B magnesium alloy. Materials Science & Engineering A: Structural Materials: Properties, Microstructure and Processing, 2008, 472, 179-186.	2.6	307
7	Low cycle fatigue properties of an extruded AZ31 magnesium alloy. International Journal of Fatigue, 2009, 31, 726-735.	2.8	234
8	Research advances of magnesium and magnesium alloys worldwide in 2021. Journal of Magnesium and Alloys, 2022, 10, 863-898.	5.5	224
9	Recent Advances in Friction Stir Welding/Processing of Aluminum Alloys: Microstructural Evolution and Mechanical Properties. Critical Reviews in Solid State and Materials Sciences, 2018, 43, 269-333.	6.8	223
10	Microstructure and fracture characteristics of spot-welded DP600 steel. Materials Science & Engineering A: Structural Materials: Properties, Microstructure and Processing, 2008, 485, 334-346.	2.6	178
11	Strain controlled cyclic deformation behavior of an extruded magnesium alloy. Materials Science & Engineering A: Structural Materials: Properties, Microstructure and Processing, 2008, 496, 106-113.	2.6	161
12	Microstructure and mechanical properties of laser welded dissimilar DP600/DP980 dual-phase steel joints. Journal of Alloys and Compounds, 2011, 509, 982-989.	2.8	160
13	Deformation and strengthening mechanisms of a carbon nanotube reinforced aluminum composite. Carbon, 2016, 104, 64-77.	5.4	156
14	A new grain orientation spread approach to analyze the dynamic recrystallization behavior of a cast-homogenized Mg-Zn-Zr alloy using electron backscattered diffraction. Materials Science & Engineering A: Structural Materials: Properties, Microstructure and Processing, 2018, 709, 285-289.	2.6	154
15	Microstructure and mechanical properties of laser welded DP600 steel joints. Materials Science & Engineering A: Structural Materials: Properties, Microstructure and Processing, 2010, 527, 1215-1222.	2.6	153
16	Effect of strain ratio and strain rate on low cycle fatigue behavior of AZ31 wrought magnesium alloy. Materials Science & Engineering A: Structural Materials: Properties, Microstructure and Processing, 2009, 517, 334-343.	2.6	141
17	Tensile properties of a friction stir welded magnesium alloy: Effect of pin tool thread orientation and weld pitch. Materials Science & Engineering A: Structural Materials: Properties, Microstructure and Processing, 2010, 527, 6064-6075.	2.6	140
18	Strain-Controlled Low-Cycle Fatigue Properties of a Newly Developed Extruded Magnesium Alloy. Metallurgical and Materials Transactions A: Physical Metallurgy and Materials Science, 2008, 39, 3014-3026.	1.1	134

#	Article	IF	CITATIONS
19	Shearing of γ″ precipitates and formation of planar slip bands in Inconel 718 during cyclic deformation. Scripta Materialia, 2005, 52, 603-607.	2.6	117
20	Dynamic recrystallization of titanium: Effect of pre-activated twinning at cryogenic temperature. Acta Materialia, 2018, 154, 311-324.	3.8	117
21	Hot deformation behavior of Ti-6Al-4V alloy: Effect of initial microstructure. Journal of Alloys and Compounds, 2017, 718, 170-181.	2.8	116
22	Detwinning and strain hardening of an extruded magnesium alloy during compression. Scripta Materialia, 2012, 67, 165-168.	2.6	113
23	Tensile and fatigue properties of a cast aluminum alloy with Ti, Zr and V additions. Materials Science & Engineering A: Structural Materials: Properties, Microstructure and Processing, 2011, 528, 8128-8138.	2.6	112
24	Tensile and fatigue properties of fiber laser welded high strength low alloy and DP980 dual-phase steel joints. Materials & Design, 2013, 43, 373-383.	5.1	112
25	Microstructure and Cyclic Deformation Behavior of a Friction-Stir-Welded 7075 Al Alloy. Metallurgical and Materials Transactions A: Physical Metallurgy and Materials Science, 2010, 41, 957-971.	1.1	111
26	Effect of heat treatment on mechanical properties of Ti–6Al–4V ELI alloy. Materials Science & Engineering A: Structural Materials: Properties, Microstructure and Processing, 2009, 506, 117-124.	2.6	109
27	Microstructural evolution and high-temperature oxidation mechanisms of a titanium aluminide based alloy. Acta Materialia, 2018, 148, 300-310.	3.8	109
28	Influence of ultrasonic spot welding on microstructure in a magnesium alloy. Scripta Materialia, 2011, 65, 911-914.	2.6	106
29	Polishing-assisted galvanic corrosion in the dissimilar friction stir welded joint of AZ31 magnesium alloy to 2024 aluminum alloy. Materials Characterization, 2009, 60, 370-376.	1.9	105
30	Tensile properties and strain-hardening behavior of double-sided arc welded and friction stir welded AZ31B magnesium alloy. Materials Science & Engineering A: Structural Materials: Properties, Microstructure and Processing, 2010, 527, 2951-2961.	2.6	105
31	Effect of annealing on interface microstructures and tensile properties of rolled Al/Mg/Al tri-layer clad sheets. Materials Science & Engineering A: Structural Materials: Properties, Microstructure and Processing, 2013, 587, 344-351.	2.6	103
32	Effect of zinc interlayer on ultrasonic spot welded aluminum-to-copper joints. Materials Science & Engineering A: Structural Materials: Properties, Microstructure and Processing, 2014, 607, 277-286.	2.6	103
33	Lap shear strength and fatigue behavior of friction stir spot welded dissimilar magnesium-to-aluminum joints with adhesive. Materials Science & Engineering A: Structural Materials: Properties, Microstructure and Processing, 2013, 562, 53-60.	2.6	97
34	Improvements of strength and ductility in aluminum alloy joints via rapid cooling during friction stir welding. Materials Science & Engineering A: Structural Materials: Properties, Microstructure and Processing, 2012, 548, 89-98.	2.6	96
35	Strengthening mechanisms in magnesium alloys containing ternary I, W and LPSO phases. Journal of Materials Science and Technology, 2018, 34, 1110-1118.	5.6	95
36	Lap shear strength and fatigue life of friction stir spot welded AZ31 magnesium and 5754 aluminum alloys. Materials Science & Engineering A: Structural Materials: Properties, Microstructure and Processing, 2012, 556, 500-509.	2.6	94

#	Article	IF	CITATIONS
37	A model for predicting the particle size dependence of the low cycle fatigue life in discontinuously reinforced MMCs. Scripta Materialia, 2004, 51, 863-867.	2.6	93
38	Mechanical properties of crossed-lamellar structures in biological shells: A review. Journal of the Mechanical Behavior of Biomedical Materials, 2017, 74, 54-71.	1.5	87
39	Strain Hardening and Strain-Rate Sensitivity of an Extruded Magnesium Alloy. Journal of Materials Engineering and Performance, 2008, 17, 894-901.	1.2	85
40	A Unified Model for the Prediction of Yield Strength in Particulate-Reinforced Metal Matrix Nanocomposites. Materials, 2015, 8, 5138-5153.	1.3	85
41	Microstructure and Low-Cycle Fatigue of a Friction-Stir-Welded 6061 Aluminum Alloy. Metallurgical and Materials Transactions A: Physical Metallurgy and Materials Science, 2010, 41, 2626-2641.	1.1	84
42	Microstructure and mechanical properties of dissimilar welded Mg–Al joints by ultrasonic spot welding technique. Science and Technology of Welding and Joining, 2012, 17, 202-206.	1.5	84
43	Microstructure and fatigue performance of single and multiple linear fiber laser welded DP980 dual-phase steel. Materials Science & Engineering A: Structural Materials: Properties, Microstructure and Processing, 2012, 553, 51-58.	2.6	84
44	Friction Stir Welded AZ31 Magnesium Alloy: Microstructure, Texture, and Tensile Properties. Metallurgical and Materials Transactions A: Physical Metallurgy and Materials Science, 2013, 44, 323-336.	1.1	84
45	Microstructure and fatigue properties of fiber laser welded dissimilar joints between high strength low alloy and dual-phase steels. Materials & Design, 2013, 51, 665-675.	5.1	82
46	Low cycle fatigue of a rare-earth containing extruded magnesium alloy. Materials Science & Engineering A: Structural Materials: Properties, Microstructure and Processing, 2013, 575, 65-73.	2.6	80
47	Improving weld strength of magnesium to aluminium dissimilar joints via tin interlayer during ultrasonic spot welding. Science and Technology of Welding and Joining, 2012, 17, 342-347.	1.5	76
48	Microstructure and mechanical properties of ultrasonic spot welded copper-to-magnesium alloy joints. Materials and Design, 2015, 84, 261-269.	3.3	75
49	Hot deformation and processing map of an as-extruded Mg–Zn–Mn–Y alloy containing I and W phases. Materials and Design, 2015, 87, 245-255.	3.3	74
50	Ageing characteristics and high-temperature tensile properties of Al–Si–Cu–Mg alloys with micro-additions of Cr, Ti, V and Zr. Materials Science & Engineering A: Structural Materials: Properties, Microstructure and Processing, 2016, 652, 353-364.	2.6	73
51	Microstructure and Mechanical Properties of Fiber-Laser-Welded and Diode-Laser-Welded AZ31 Magnesium Alloy. Metallurgical and Materials Transactions A: Physical Metallurgy and Materials Science, 2011, 42, 1974-1989.	1.1	70
52	Effect of rare earth elements on deformation behavior of an extruded Mg–10Gd–3Y–0.5Zr alloy during compression. Materials & Design, 2013, 46, 411-418.	5.1	70
53	Dependence of the distribution of deformation twins on strain amplitudes in an extruded magnesium alloy after cyclic deformation. Materials Science & Engineering A: Structural Materials: Properties, Microstructure and Processing, 2009, 519, 38-45.	2.6	69
54	Exfoliation corrosion of friction stir welded dissimilar 2024-to-7075 aluminum alloys. Materials Characterization, 2019, 147, 93-100.	1.9	69

#	Article	IF	CITATIONS
55	Relationship between fractal dimension and fatigue threshold value in dual-phase steels. Scripta Metallurgica, 1988, 22, 827-832.	1.2	68
56	Microstructure and tensile properties of thixomolded magnesium alloys. Journal of Alloys and Compounds, 2010, 496, 140-148.	2.8	68
57	Microstructure and mechanical properties of weld-bonded and resistance spot welded magnesium-to-steel dissimilar joints. Materials Science & Engineering A: Structural Materials: Properties, Microstructure and Processing, 2012, 537, 11-24.	2.6	68
58	Characterization of hot deformation behavior of an extruded Mg–Zn–Mn–Y alloy containing LPSO phase. Journal of Alloys and Compounds, 2015, 644, 814-823.	2.8	68
59	Fatigue behavior of tailor (laser)-welded blanks for automotive applications. Materials Science & Engineering A: Structural Materials: Properties, Microstructure and Processing, 2006, 420, 199-207.	2.6	64
60	Strategies for enhancing the room-temperature stretch formability of magnesium alloy sheets: a review. Journal of Materials Science, 2021, 56, 12965.	1.7	64
61	Effect of boron on fatigue crack growth behavior in superalloy IN 718 at RT and 650°C. Materials Science & Engineering A: Structural Materials: Properties, Microstructure and Processing, 2006, 428, 1-11.	2.6	63
62	Tensile Properties and Work Hardening Behavior of Laser-Welded Dual-Phase Steel Joints. Journal of Materials Engineering and Performance, 2012, 21, 222-230.	1.2	62
63	Effects of aluminum content and strain rate on strain hardening behavior of cast magnesium alloys during compression. Materials Science & Engineering A: Structural Materials: Properties, Microstructure and Processing, 2014, 594, 235-245.	2.6	62
64	Dependence of compressive deformation on pre-strain and loading direction in an extruded magnesium alloy: Texture, twinning and de-twinning. Materials Science & Engineering A: Structural Materials: Properties, Microstructure and Processing, 2014, 596, 134-144.	2.6	62
65	A Critical Review of Mg–Zn–Y Series Alloys Containing I, W, and LPSO Phases. Advanced Engineering Materials, 2016, 18, 1983-2002.	1.6	62
66	Ultrasonic spot welded 6111-T4 aluminum alloy to galvanized high-strength low-alloy steel: Microstructure and mechanical properties. Materials and Design, 2017, 113, 284-296.	3.3	62
67	Toughening mechanisms in iron-containing hydroxyapatite/titanium composites. Biomaterials, 2010, 31, 1493-1501.	5.7	61
68	Tensile properties of AZ61 magnesium alloy produced by multi-pass friction stir processing: Effect of sample orientation. Materials Science & Engineering A: Structural Materials: Properties, Microstructure and Processing, 2018, 725, 398-405.	2.6	61
69	Liquid metal embrittlement in laser beam welding of Zn-coated 22MnB5 steel. Materials and Design, 2018, 155, 375-383.	3.3	61
70	Cyclic deformation behavior of a cast aluminum alloy. Materials Science & Engineering A: Structural Materials: Properties, Microstructure and Processing, 2009, 516, 31-41.	2.6	60
71	Welding behaviour, microstructure and mechanical properties of dissimilar resistance spot welds between galvannealed HSLA350 and DP600 steels. Science and Technology of Welding and Joining, 2009, 14, 616-625.	1.5	58
72	Ultrasonic Spot Welding of Aluminum to High-Strength Low-Alloy Steel: Microstructure, Tensile and Fatigue Properties. Metallurgical and Materials Transactions A: Physical Metallurgy and Materials Science, 2014, 45, 2055-2066.	1.1	58

#	Article	IF	CITATIONS
73	Effect of welding energy on microstructure and strength of ultrasonic spot welded dissimilar joints of aluminum to steel sheets. Materials Science & Engineering A: Structural Materials: Properties, Microstructure and Processing, 2016, 668, 73-85.	2.6	58
74	Influence of microstructural evolution on tensile properties of friction stir welded joint of rolled SiCp/AA2009-T351 sheet. Materials & Design, 2013, 51, 199-205.	5.1	57
75	Microstructure and fatigue properties of Mg-to-steel dissimilar resistance spot welds. Materials & Design, 2013, 45, 336-342.	5.1	57
76	Formation of zinc interlayer texture during dissimilar ultrasonic spot welding of magnesium and high strength low alloy steel. Materials & Design, 2013, 45, 236-240.	5.1	57
77	Cyclic deformation and twinning in a semi-solid processed AZ91D magnesium alloy. Materials Science & Engineering A: Structural Materials: Properties, Microstructure and Processing, 2010, 528, 208-219.	2.6	56
78	Ultrasonic spot welded AZ31 magnesium alloy: Microstructure, texture, and lap shear strength. Materials Science & Engineering A: Structural Materials: Properties, Microstructure and Processing, 2013, 569, 78-85.	2.6	56
79	Tensile and fatigue properties of electron beam welded dissimilar joints between Ti–6Al–4V and BT9 titanium alloys. Materials Science & Engineering A: Structural Materials: Properties, Microstructure and Processing, 2013, 584, 47-56.	2.6	55
80	Ultrasonic spot welding of Al/Mg/Al tri-layered clad sheets. Materials & Design, 2014, 62, 344-351.	5.1	55
81	Carbon Nanotubeâ€Reinforced Aluminum Matrix Composites. Advanced Engineering Materials, 2020, 22, 1901176.	1.6	55
82	Expulsion monitoring in spot welded advanced high strength automotive steels. Science and Technology of Welding and Joining, 2006, 11, 480-487.	1.5	54
83	Tensile properties and strain-hardening behaviour of friction stir welded SiCp/AA2009 composite joints. Materials Science & Engineering A: Structural Materials: Properties, Microstructure and Processing, 2014, 608, 1-10.	2.6	54
84	Cyclic deformation behavior of a super-vacuum die cast magnesium alloy. Materials Science & Engineering A: Structural Materials: Properties, Microstructure and Processing, 2012, 546, 72-81.	2.6	52
85	Tensile and compressive deformation behavior of the Al–Si–Cu–Mg cast alloy with additions of Zr, V and Ti. Materials & Design, 2014, 59, 352-358.	5.1	52
86	Thermal stability of (AlSi) (ZrVTi) intermetallic phases in the Al–Si–Cu–Mg cast alloy with additions of Ti, V, and Zr. Thermochimica Acta, 2014, 595, 11-16.	1.2	52
87	Improving High-Temperature Tensile and Low-Cycle Fatigue Behavior of Al-Si-Cu-Mg Alloys Through Micro-additions of Ti, V, and Zr. Metallurgical and Materials Transactions A: Physical Metallurgy and Materials Science, 2015, 46, 3063-3078.	1.1	52
88	Residual stresses and high cycle fatigue properties of friction stir welded SiCp/AA2009 composites. International Journal of Fatigue, 2013, 55, 64-73.	2.8	51
89	Strain-controlled fatigue properties of dissimilar welded joints between Ti–6Al–4V and Ti17 alloys. Materials & Design, 2013, 49, 716-727.	5.1	51
90	Effect of Zr, V and Ti on hot compression behavior of the Al–Si cast alloy for powertrain applications. Journal of Alloys and Compounds, 2014, 615, 1019-1031.	2.8	51

#	Article	IF	CITATIONS
91	Microstructure and mechanical properties of ultrasonic spot welded Al/Ti alloy joints. Materials & Design, 2015, 78, 33-41.	5.1	51
92	Cyclic deformation mechanisms of precipitation-hardened Inconel 718 superalloy. Materials Science & Engineering A: Structural Materials: Properties, Microstructure and Processing, 2008, 483-484, 369-372.	2.6	50
93	Monotonic and cyclic deformation behavior of the Al–Si–Cu–Mg cast alloy with micro-additions of Ti, V and Zr. International Journal of Fatigue, 2015, 70, 383-394.	2.8	50
94	Effect of Mn and heat treatment on improvements in static strength and low-cycle fatigue life of an Al–Si–Cu–Mg alloy. Materials Science & Engineering A: Structural Materials: Properties, Microstructure and Processing, 2016, 657, 441-452.	2.6	50
95	Enhancing mechanical properties of AZ61 magnesium alloy via friction stir processing: Effect of processing parameters. Materials Science & Engineering A: Structural Materials: Properties, Microstructure and Processing, 2020, 797, 139945.	2.6	49
96	Microstructure and mechanical properties of Mg-to-Al dissimilar welded joints with an Ag interlayer using ultrasonic spot welding. Journal of Magnesium and Alloys, 2020, 8, 552-563.	5.5	49
97	Fatigue properties of laser welded dual-phase steel joints. Procedia Engineering, 2010, 2, 835-843.	1.2	48
98	Texture transformation in an extruded magnesium alloy under pressure. Materials Science & Engineering A: Structural Materials: Properties, Microstructure and Processing, 2013, 582, 63-67.	2.6	48
99	Work hardening and texture during compression deformation of the Al–Si–Cu–Mg alloy modified with V, Zr and Ti. Journal of Alloys and Compounds, 2014, 593, 290-299.	2.8	48
100	Texture evolution of AZ31 magnesium alloy sheets during warm rolling. Journal of Alloys and Compounds, 2015, 645, 70-77.	2.8	48
101	De-twinning and Texture Change in an Extruded AM30 Magnesium Alloy during Compression along Normal Direction. Journal of Materials Science and Technology, 2015, 31, 264-268.	5.6	47
102	Liquid metal embrittlement in laser lap joining of TWIP and medium-manganese TRIP steel: The role of stress and grain boundaries. Materials Characterization, 2018, 145, 627-633.	1.9	47
103	Microstructure and mechanical properties of Al–Si cast alloy with additions of Zr–V–Ti. Materials and Design, 2015, 83, 801-812.	3.3	46
104	Ultrasonic spot welding of rare-earth containing ZEK100 magnesium alloy to 5754 aluminum alloy. Materials Science & Engineering A: Structural Materials: Properties, Microstructure and Processing, 2016, 666, 139-148.	2.6	46
105	Contribution of the cyclic loading portion below the opening load to fatigue crack growth. Materials Science & Engineering A: Structural Materials: Properties, Microstructure and Processing, 1996, 208, 181-187.	2.6	45
106	Strain-controlled low cycle fatigue properties of a rare-earth containing ZEK100 magnesium alloy. Materials & Design, 2015, 67, 436-447.	5.1	44
107	Influence of aluminum content on twinning and texture development of cast Mg–Al–Zn alloy during compression. Journal of Alloys and Compounds, 2015, 623, 15-23.	2.8	44
108	Single and double twin nucleation, growth, and interaction in an extruded magnesium alloy. Materials and Design, 2017, 119, 376-396.	3.3	44

#	Article	IF	CITATIONS
109	Twin-twin interactions and contraction twin formation in an extruded magnesium alloy subjected to an alteration of compressive direction. Journal of Alloys and Compounds, 2018, 737, 549-560.	2.8	44
110	Fiber Laser Welded AZ31 Magnesium Alloy: The Effect of Welding Speed on Microstructure and Mechanical Properties. Metallurgical and Materials Transactions A: Physical Metallurgy and Materials Science, 2012, 43, 2133-2147.	1.1	41
111	Microstructure and Fatigue Properties of a Friction Stir Lap Welded Magnesium Alloy. Metallurgical and Materials Transactions A: Physical Metallurgy and Materials Science, 2013, 44, 3732-3746.	1.1	41
112	Characterization of ultrasonic spot welded joints of Mg-to-galvanized and ungalvanized steel with a tin interlayer. Journal of Materials Processing Technology, 2014, 214, 811-817.	3.1	41
113	Effect of strain rate and temperature on strain hardening behavior of a dissimilar joint between Ti–6Al–4V and Ti17 alloys. Materials & Design, 2014, 56, 174-184.	5.1	41
114	Ageing characteristics and high-temperature tensile properties of Al–Si–Cu–Mg alloys with micro-additions of Mo and Mn. Materials Science & Engineering A: Structural Materials: Properties, Microstructure and Processing, 2017, 684, 726-736.	2.6	41
115	Influence of yttrium content on phase formation and strain hardening behavior of Mg–Zn–Mn magnesium alloy. Journal of Alloys and Compounds, 2014, 615, 424-432.	2.8	40
116	Twin Growth and Texture Evolution in an Extruded AM30 Magnesium Alloy During Compression. Journal of Materials Science and Technology, 2014, 30, 884-887.	5.6	40
117	Tensile and fatigue behavior of electron beam welded dissimilar joints of Ti–6Al–4V and IMI834 titanium alloys. Materials Science & Engineering A: Structural Materials: Properties, Microstructure and Processing, 2016, 649, 146-152.	2.6	40
118	Hot deformation and activation energy of a CNT-reinforced aluminum matrix nanocomposite. Materials Science & Engineering A: Structural Materials: Properties, Microstructure and Processing, 2017, 695, 322-331.	2.6	40
119	Modeling dynamic recrystallization during hot deformation of a cast-homogenized Mg-Zn-Zr alloy. Materials Science & Engineering A: Structural Materials: Properties, Microstructure and Processing, 2018, 720, 180-188.	2.6	40
120	Fatigue crack growth behavior of X2095 Al–Li alloy. International Journal of Fatigue, 1999, 21, 1079-1086.	2.8	39
121	Low cycle fatigue behavior of a semi-solid processed AM60B magnesium alloy. Materials & Design, 2013, 49, 456-464.	5.1	39
122	Effect of Ti on the wear behavior of AlCoCrFeNi high-entropy alloy during unidirectional and bi-directional sliding wear processes. Wear, 2021, 476, 203650.	1.5	38
123	Low-cycle fatigue of a friction stir welded 2219-T62 aluminum alloy at different welding parameters and cooling conditions. International Journal of Advanced Manufacturing Technology, 2014, 74, 209-218.	1.5	37
124	Effects of concavity on tensile and fatigue properties in fibre laser welding of automotive steels. Science and Technology of Welding and Joining, 2014, 19, 60-68.	1.5	37
125	Bimodal grain microstructure development during hot compression of a cast-homogenized Mg-Zn-Zr alloy. Materials Science & Engineering A: Structural Materials: Properties, Microstructure and Processing, 2018, 724, 421-430.	2.6	37
126	Three-dimensional fractal analysis of fracture surfaces in a titanium alloy for biomedical applications. Scripta Materialia, 2008, 59, 391-394.	2.6	36

#	Article	lF	CITATIONS
127	Hot Deformation and Work Hardening Behavior of an Extruded Mg–Zn–Mn–Y Alloy. Journal of Materials Science and Technology, 2015, 31, 1161-1170.	5.6	36
128	A new geometric factor formula for a center cracked plate tensile specimen of finite width. International Journal of Fracture, 1992, 55, R3-R8.	1.1	35
129	Influence of pre-strain on de-twinning activity in an extruded AM30 magnesium alloy. Materials Science & Engineering A: Structural Materials: Properties, Microstructure and Processing, 2014, 605, 73-79.	2.6	35
130	Effect of pin tool thread orientation on fatigue strength of friction stir welded AZ31B-H24 Mg butt joints. Procedia Engineering, 2010, 2, 825-833.	1.2	34
131	Influence of pre-deformation and subsequent annealing on strain hardening and anisotropy of AM30 magnesium alloy. Journal of Alloys and Compounds, 2014, 611, 341-350.	2.8	34
132	Microstructure and Mechanical Properties of an Ultrasonic Spot Welded Aluminum Alloy: The Effect of Welding Energy. Materials, 2017, 10, 449.	1.3	34
133	Multi-pass submerged friction stir processing of AZ61 magnesium alloy: strengthening mechanisms and fracture behavior. Journal of Materials Science, 2019, 54, 8640-8654.	1.7	34
134	A model for crack closure. Engineering Fracture Mechanics, 1996, 53, 493-509.	2.0	33
135	Fatigue of rareâ€earth containing magnesium alloys: a review. Fatigue and Fracture of Engineering Materials and Structures, 2014, 37, 831-853.	1.7	33
136	Low cycle fatigue properties of friction stir welded joints of a semi-solid processed AZ91D magnesium alloy. Materials & Design, 2014, 56, 1-8.	5.1	33
137	Low cycle fatigue of an extruded Mg–3Nd–0.2Zn–0.5Zr magnesium alloy. Materials & Design, 2014, 64, 63-73.	5.1	32
138	Microstructure, tensile and fatigue properties of ultrasonic spot welded aluminum to galvanized high-strength-low-alloy and low-carbon steel sheets. Materials Science & Engineering A: Structural Materials: Properties, Microstructure and Processing, 2017, 690, 323-336.	2.6	32
139	Effect of strain ratio on cyclic deformation behavior of a rare-earth containing extruded magnesium alloy. Materials Science & Engineering A: Structural Materials: Properties, Microstructure and Processing, 2013, 588, 250-259.	2.6	31
140	Heat Treatment Development for a Rapidly Solidified Heat Resistant Cast Al-Si Alloy. Journal of Materials Engineering and Performance, 2013, 22, 1839-1847.	1.2	31
141	Tensile properties of fiber laser welded joints of high strength low alloy and dual-phase steels at warm and low temperatures. Materials & Design, 2014, 56, 193-199.	5.1	31
142	Strain-controlled fatigue properties of linear friction welded dissimilar joints between Ti–6Al–4V and Ti–6.5Al–3.5Mo–1.5Zr–0.3Si alloys. Materials Science & Engineering A: Structural Materials: Properties, Microstructure and Processing, 2014, 612, 80-88.	2.6	31
143	The dependence of near-threshold fatigue crack growth on microstructure and environment in dual-phase steels. Materials Science & Engineering A: Structural Materials: Properties, Microstructure and Processing, 1989, 108, 141-151.	2.6	30
144	Effect of boron on the low-cycle fatigue behavior and deformation structure of INCONEL 718 at 650 °C. Metallurgical and Materials Transactions A: Physical Metallurgy and Materials Science, 2004, 35, 3477-3487.	1.1	30

#	Article	IF	CITATIONS
145	Effect of Boron and Carbon on the Fracture Toughness of IN 718 Superalloy at Room Temperature and 650 °C. Journal of Materials Engineering and Performance, 2005, 14, 528-538.	1.2	30
146	Low-cycle fatigue behavior of INCONEL 718 superalloy with different concentrations of boron at room temperature. Metallurgical and Materials Transactions A: Physical Metallurgy and Materials Science, 2005, 36, 2671-2684.	1.1	29
147	Cyclic deformation of dissimilar welded joints between Ti–6Al–4V and Ti17 alloys: Effect of strain ratio. Materials Science & Engineering A: Structural Materials: Properties, Microstructure and Processing, 2014, 598, 122-134.	2.6	29
148	Cyclic Deformation Behavior of a Rare-Earth Containing Extruded Magnesium Alloy: Effect of Heat Treatment. Metallurgical and Materials Transactions A: Physical Metallurgy and Materials Science, 2015, 46, 1168-1187.	1.1	29
149	Low cycle fatigue of SiCp reinforced AA2009 composites. Materials & Design, 2015, 66, 274-283.	5.1	29
150	Effect of Cr, Ti, V, and Zr Micro-additions on Microstructure and Mechanical Properties of the Al-Si-Cu-Mg Cast Alloy. Metallurgical and Materials Transactions A: Physical Metallurgy and Materials Science, 2016, 47, 2396-2409.	1.1	29
151	Ultrasonic Spot Welding of a Rare-Earth Containing ZEK100 Magnesium Alloy: Effect of Welding Energy. Metallurgical and Materials Transactions A: Physical Metallurgy and Materials Science, 2016, 47, 1686-1697.	1.1	29
152	Strain hardening behavior and mechanisms of friction stir welded dissimilar joints of aluminum alloys. Materials Letters, 2018, 231, 68-71.	1.3	29
153	Ultrasonic spot welding of magnesium-to-aluminum alloys with a copper interlayer: Microstructural evolution and tensile properties. Journal of Manufacturing Processes, 2019, 37, 91-100.	2.8	29
154	Resistance spot weld fatigue behavior and dislocation substructures in two different heats of AZ31 magnesium alloy. Materials Science & Engineering A: Structural Materials: Properties, Microstructure and Processing, 2011, 529, 81-87.	2.6	28
155	Zirconium nitride nano-particulate reinforced Alon composites: Fabrication, mechanical properties and toughening mechanisms. Journal of the European Ceramic Society, 2011, 31, 883-892.	2.8	28
156	Tensile and fatigue properties of weld-bonded and adhesive-bonded magnesium alloy joints. Materials Science & Engineering A: Structural Materials: Properties, Microstructure and Processing, 2013, 563, 125-132.	2.6	28
157	Influence of Test Temperature on the Tensile Properties along the Thickness in a Friction Stir Welded Aluminum Alloy. Journal of Materials Science and Technology, 2015, 31, 953-961.	5.6	28
158	Microstructure and low cycle fatigue of a Ti2AlNb-based lightweight alloy. Journal of Materials Science and Technology, 2020, 44, 140-147.	5.6	28
159	Effects of welding and weld heat-affected zone simulation on the microstructure and mechanical behavior of a 2195 aluminum-lithium alloy. Metallurgical and Materials Transactions A: Physical Metallurgy and Materials Science, 2001, 32, 2729-2741.	1.1	27
160	Effect of solidification rate and loading mode on deformation behavior of cast Al–Si–Cu–Mg alloy with additions of transition metals. Materials Science & Engineering A: Structural Materials: Properties, Microstructure and Processing, 2015, 636, 361-372.	2.6	27
161	Ultrasonic spot welding of 5182 aluminum alloy: Evolution of microstructure and mechanical properties. Materials Science & amp; Engineering A: Structural Materials: Properties, Microstructure and Processing, 2019, 756, 417-429.	2.6	27
162	Near-threshold fatigue crack growth behavior of 2195 aluminum-lithium-alloy—prediction of crack propagation direction and influence of stress ratio. Metallurgical and Materials Transactions A: Physical Metallurgy and Materials Science, 2000, 31, 1531-1541.	1.1	26

#	Article	IF	CITATIONS
163	Change of microstructure and cyclic deformation behavior along the thickness in a friction-stir-welded aluminum alloy. Scripta Materialia, 2012, 66, 5-8.	2.6	26
164	Fatigue life estimation of ultrasonic spot welded Mg alloy joints. Materials & Design, 2014, 62, 124-132.	5.1	26
165	Cymbiola nobilis shell: Toughening mechanisms in a crossed-lamellar structure. Scientific Reports, 2017, 7, 40043.	1.6	26
166	Electromagnetic pulse welding of Al/Cu dissimilar materials: Microstructure and tensile properties. Materials Science & Engineering A: Structural Materials: Properties, Microstructure and Processing, 2020, 792, 139842.	2.6	26
167	A new evaluation procedure for crack closure. International Journal of Fatigue, 1991, 13, 327-331.	2.8	25
168	Effect of specimen orientation and welding on the fracture and fatigue properties of 2195 Al–Li alloy. Materials Science & Engineering A: Structural Materials: Properties, Microstructure and Processing, 2004, 387-389, 465-469.	2.6	25
169	Etching technique for revelation of plastic deformation zone in low carbon steel. Materials Science and Technology, 2005, 21, 530-538.	0.8	25
170	Microstructure and Strain Hardening of a Friction Stir Welded High-Strength Al–Zn–Mg Alloy. Acta Metallurgica Sinica (English Letters), 2014, 27, 723-729.	1.5	25
171	Interfacial Characterization of Dissimilar Joints Between Al/Mg/Al-Trilayered Clad Sheet to High-Strength Low-Alloy Steel. Jom, 2015, 67, 1468-1477.	0.9	25
172	Microstructure and Mechanical Properties of Ultrasonic Spot Welded Mg/Al Alloy Dissimilar Joints. Metals, 2018, 8, 229.	1.0	25
173	Cyclic deformation behavior of friction-stir-welded dissimilar AA5083-to-AA2024 joints: Effect of microstructure and loading history. Materials Science & Engineering A: Structural Materials: Properties, Microstructure and Processing, 2019, 744, 145-153.	2.6	25
174	Multiple α sub-variants and anisotropic mechanical properties of an additively-manufactured Ti-6Al-4V alloy. Journal of Materials Science and Technology, 2021, 70, 113-124.	5.6	25
175	The effective fatigue threshold: significance of the loading cycle below the crack opening load. International Journal of Fatigue, 1994, 16, 485-491.	2.8	24
176	Cyclic deformation behavior of linear friction welded Ti6Al4V joints. Materials Science & Engineering A: Structural Materials: Properties, Microstructure and Processing, 2014, 597, 408-414.	2.6	24
177	Strain-controlled low cycle fatigue properties of a rare-earth containing ME20 magnesium alloy. Materials Science & Engineering A: Structural Materials: Properties, Microstructure and Processing, 2016, 661, 115-125.	2.6	24
178	Three-dimensional processing maps and microstructural evolution of a CNT-reinforced Al-Cu-Mg nanocomposite. Materials Science & Engineering A: Structural Materials: Properties, Microstructure and Processing, 2017, 702, 425-437.	2.6	24
179	Heterogeneous microstructure and deformation behavior of an automotive grade aluminum alloy. Journal of Alloys and Compounds, 2021, 870, 159413.	2.8	24
180	Determination of volume fraction of bainite in low carbon steels using artificial neural networks. Computational Materials Science, 2011, 50, 3377-3384.	1.4	23

#	Article	IF	CITATIONS
181	Material flow and core/multi-shell structures in a friction stir welded aluminum alloy with embedded copper markers. Journal of Alloys and Compounds, 2011, 509, 8449-8454.	2.8	23
182	An improved model for bainite formation at isothermal temperatures. Scripta Materialia, 2011, 64, 73-76.	2.6	23
183	Deformation behavior and strengthening mechanisms in a CNT-reinforced bimodal-grained aluminum matrix nanocomposite. Materials Science & Engineering A: Structural Materials: Properties, Microstructure and Processing, 2021, 817, 141370.	2.6	23
184	Microstructural evolution and enhanced mechanical properties of Mg–Gd–Y–Zn–Zr alloy via centrifugal casting, ring-rolling and aging. Journal of Magnesium and Alloys, 2022, 10, 119-128.	5.5	23
185	Effect of stress ratio and loading condition on the fatigue threshold. International Journal of Fatigue, 1992, 14, 325-329.	2.8	22
186	THE ELECTRON CHANNELLING CONTRAST TECHNIQUE APPLIED TO THE CHARACTERISATION OF DISLOCATION STRUCTURES IN THE VICINITY OF A FATIGUE CRACK. Fatigue and Fracture of Engineering Materials and Structures, 1997, 20, 1551-1561.	1.7	22
187	Investigation of macro deformation bands in fatigued [001] Cu single crystals by electron channeling contrast technique. Scripta Materialia, 1997, 37, 1605-1610.	2.6	22
188	Effect of boron and carbon on thermomechanical fatigue of IN 718 superalloy. Materials Science & Engineering A: Structural Materials: Properties, Microstructure and Processing, 2006, 437, 157-171.	2.6	22
189	Microstructural Evaluation of Friction Stir Processed AZ31B-H24 Magnesium Alloy. Canadian Metallurgical Quarterly, 2007, 46, 425-432.	0.4	22
190	Microstructure and cyclic deformation behavior of a 3D-printed Ti–6Al–4V alloy. Journal of Alloys and Compounds, 2020, 825, 153971.	2.8	22
191	A new approach for the determination of stress intensity factors for finite width plate. Engineering Fracture Mechanics, 1994, 48, 561-571.	2.0	21
192	Three-dimensional fractal analysis of fracture surfaces in titanium–iron particulate reinforced hydroxyapatite composites: relationship between fracture toughness and fractal dimension. Journal of Materials Science, 2011, 46, 6118-6123.	1.7	21
193	Dislocation slip distance during compression of Al–Si–Cu–Mg alloy with additions of Ti–Zr–V. Materials Science and Technology, 2015, 31, 63-72.	0.8	21
194	Solid-state ultrasonic spot welding of SiCp/2009Al composite sheets. Materials & Design, 2015, 65, 489-495.	5.1	21
195	Low cycle fatigue properties of friction stir welded dissimilar 2024-to-7075 aluminum alloy joints. Materials Science & Engineering A: Structural Materials: Properties, Microstructure and Processing, 2022, 832, 142423.	2.6	21
196	A modified Johnson-Cook constitutive relationship for a rare-earth containing magnesium alloy. Journal of Rare Earths, 2013, 31, 1202-1207.	2.5	20
197	Effect of transition metals on energy absorption during strain-controlled fatigue of an aluminum alloy. International Journal of Fatigue, 2016, 87, 456-470.	2.8	20
198	Thermodynamic and microstructural study of Ti2AlNb oxides at 800 °C. Scientific Reports, 2018, 8, 12761.	1.6	20

#	Article	IF	CITATIONS
199	A model for the low cycle fatigue life prediction of discontinuously reinforced MMCs. International Journal of Fatigue, 2005, 27, 417-427.	2.8	19
200	Prediction of fracture strength in Al2O3/SiCpceramic matrix nanocomposites. Science and Technology of Advanced Materials, 2007, 8, 5-10.	2.8	19
201	Microstructural evolution and mechanical properties of electron beam welded dissimilar titanium alloy joints. Materials Science & Engineering A: Structural Materials: Properties, Microstructure and Processing, 2017, 697, 224-232.	2.6	19
202	Microstructure and mechanical properties of Mg/Mg bimetal composites fabricated by hot-pressing diffusion and co-extrusion. Materials Science & Engineering A: Structural Materials: Properties, Microstructure and Processing, 2019, 764, 138194.	2.6	19
203	Kinking and cracking behavior in nacre under stepwise compressive loading. Materials Science and Engineering C, 2020, 108, 110364.	3.8	19
204	Natural arrangement of fiber-like aragonites and its impact on mechanical behavior of mollusk shells: A review. Journal of the Mechanical Behavior of Biomedical Materials, 2020, 110, 103940.	1.5	19
205	Thermal shock behavior of nano-sized SiC particulate reinforced AlON composites. Materials Science and Engineering B: Solid-State Materials for Advanced Technology, 2012, 177, 402-410.	1.7	18
206	Texture Development in a Friction Stir Lap-Welded AZ31B Magnesium Alloy. Metallurgical and Materials Transactions A: Physical Metallurgy and Materials Science, 2014, 45, 4333-4349.	1.1	18
207	Cyclic deformation and anelastic behavior of ZEK100 magnesium alloy: Effect of strain ratio. Materials Science & Engineering A: Structural Materials: Properties, Microstructure and Processing, 2015, 640, 243-258.	2.6	18
208	Correlating Hardness Retention and Phase Transformations of Al and Mg Cast Alloys for Aerospace Applications. Journal of Materials Engineering and Performance, 2015, 24, 1365-1378.	1.2	18
209	Texture evolution and deformation activity of an extruded magnesium alloy: Effect of yttrium and deformation temperature. Journal of Alloys and Compounds, 2016, 688, 270-284.	2.8	18
210	Microstructure and Fatigue Properties of Ultrasonic Spot Welded Joints of Aluminum 5754 Alloy. Jom, 2016, 68, 1465-1475.	0.9	18
211	Experimental study of the effect of loading condition on fracture surface contact features and crack closure behavior in a carbon steel. Engineering Fracture Mechanics, 2006, 73, 1117-1132.	2.0	17
212	Modeling the dependence of strength on grain sizes in nanocrystalline materials. Science and Technology of Advanced Materials, 2008, 9, 015003.	2.8	16
213	Resistance Spot Welding Characteristics and Mechanical Properties of Galvannealed HSLA 350 Steel. Canadian Metallurgical Quarterly, 2009, 48, 303-310.	0.4	16
214	Dissimilar ultrasonic spot welding of Mg-Al and Mg-high strength low alloy steel. Theoretical and Applied Mechanics Letters, 2014, 4, 041005.	1.3	16
215	Low ycle fatigue behavior of a newly developed cast aluminum alloy for automotive applications. Fatigue and Fracture of Engineering Materials and Structures, 2019, 42, 1912-1926.	1.7	16
216	Silicon nitride composites with magnesia and alumina additives: Toughening mechanisms and mechanical properties. Materials Science & Engineering A: Structural Materials: Properties, Microstructure and Processing, 2020, 779, 139140.	2.6	16

#	Article	IF	CITATIONS
217	Achieving superior mechanical properties in a low-alloyed magnesium alloy via low-temperature extrusion. Materials Science & Engineering A: Structural Materials: Properties, Microstructure and Processing, 2022, 851, 143611.	2.6	16
218	Effect of coating on fiber laser welded joints of DP980 steels. Materials and Design, 2016, 90, 516-523.	3.3	15
219	Ultrasonic spot welding of a clad 7075 aluminum alloy: Strength and fatigue life. International Journal of Fatigue, 2020, 141, 105869.	2.8	15
220	Fracture toughness of Si3N4 ceramic composites: Effect of texture. Journal of the European Ceramic Society, 2021, 41, 6346-6355.	2.8	15
221	Effect of Welding Parameters on Microstructure and Tensile Properties of Friction Stir Welded 6061 AL Joints. Materials Science Forum, 0, 618-619, 41-44.	0.3	14
222	Flat-Cladding Fiber Bragg Grating Sensors for Large Strain Amplitude Fatigue Tests. Sensors, 2010, 10, 7674-7680.	2.1	14
223	Development and experimental validation of a neural network model for prediction and analysis of the strength of bainitic steels. Materials & Design, 2012, 41, 99-107.	5.1	14
224	Residual stresses in suspension plasma sprayed electrolytes in metal-supported solid oxide fuel cell half cells. Journal of Power Sources, 2013, 221, 397-405.	4.0	14
225	Microstructure, hardness, and fracture toughness of suspension plasma sprayed yttria-stabilized zirconia electrolytes on stainless steel substrates. Thin Solid Films, 2015, 584, 23-28.	0.8	14
226	Cyclic deformation behavior of a high zinc-containing cast magnesium alloy. International Journal of Fatigue, 2019, 125, 1-10.	2.8	14
227	Flow, process forces and strains during Friction Stir Welding: A comprehensive First principle approach. Proceedings of the Institution of Mechanical Engineers, Part B: Journal of Engineering Manufacture, 2021, 235, 912-924.	1.5	14
228	An Analytical Model for Predicting the Yield Strength of Particulate-Reinforced Metal Matrix Nanocomposites with Consideration of Porosity. Nanoscience and Nanotechnology Letters, 2012, 4, 794-800.	0.4	14
229	Numerical assessment of stress distribution ahead of the crack tip for finite-width center cracked tension specimen. International Journal of Fracture, 1993, 63, R67-R74.	1.1	13
230	Determination of precise geometric correction factor regarding stress intensity by a "force balance method― International Journal of Fracture, 1993, 59, R53-R57.	1.1	13
231	Oxidation behaviour of nano-sized SiC particulate reinforced Alon composites. Journal of the European Ceramic Society, 2011, 31, 2255-2265.	2.8	13
232	Corrosion of aluminum oxynitride based ceramics by molten steel. Ceramics International, 2013, 39, 3049-3054.	2.3	13
233	SiC and ZrN nano-particulate reinforced AlON composites: Preparation, mechanical properties and toughening mechanisms. Ceramics International, 2016, 42, 6072-6079.	2.3	13
234	Linear Friction Welding of Dissimilar Materials 316L Stainless Steel to Zircaloy-4. Metallurgical and Materials Transactions A: Physical Metallurgy and Materials Science, 2018, 49, 1641-1652.	1.1	13

#	Article	IF	CITATIONS
235	A geometric correction function for a finite width center cracked plate loaded by a pair of splitting forces. International Journal of Fracture, 1992, 56, R19-R22.	1.1	12
236	An in-vitro Investigation of Iron-Containing Hydroxyapatite/Titanium Composites. Journal of Materials Science and Technology, 2011, 27, 546-552.	5.6	12
237	Mechanical properties and toughening mechanisms of silicon carbide nano-particulate reinforced Alon composites. Materials Science & Engineering A: Structural Materials: Properties, Microstructure and Processing, 2012, 538, 118-124.	2.6	12
238	Core-multishell globular oxidation in a new TiAlNbCr alloy at high temperatures. Scientific Reports, 2017, 7, 3483.	1.6	12
239	Microstructure and fatigue properties of linear friction welded TC4 titanium alloy joints. Science and Technology of Welding and Joining, 2017, 22, 177-181.	1.5	12
240	A self-assembled smart architecture against drilling predation in a Pinctada maxima shell: protective mechanisms. Journal of Materials Science, 2018, 53, 3417-3426.	1.7	12
241	High-temperature tensile behavior of AZ61 magnesium plate prepared by multi-pass friction stir processing. Materials Science & Engineering A: Structural Materials: Properties, Microstructure and Processing, 2019, 759, 234-240.	2.6	12
242	Determination of precise geometric correction factor regarding stress intensity by a ?force balance method?. International Journal of Fracture, 1993, 59, R53-R57.	1.1	11
243	Thermal shock behavior of nano-sized ZrN particulate reinforced AlON composites. Ceramics International, 2013, 39, 367-375.	2.3	11
244	The role of minor yttrium in tailoring the failure resistance of surface oxide film formed on Mg alloys. Thin Solid Films, 2016, 615, 29-37.	0.8	11
245	Tribological properties of AZ31 alloy pre-deformed at low and high strain rates via the work function. Wear, 2018, 414-415, 126-135.	1.5	11
246	High-temperature oxidation mechanisms of nano-/submicro-scale lamellar structures in an intermetallic alloy. Scripta Materialia, 2019, 171, 102-107.	2.6	11
247	Oxidation mechanisms of an intermetallic alloy at high temperatures. Scripta Materialia, 2021, 199, 113852.	2.6	11
248	Compressive deformation behaviour and toughening mechanisms of spark plasma sintered NiAl-CNT composites. Ceramics International, 2022, 48, 16072-16084.	2.3	11
249	Near-threshold corrosion fatigue crack growth in dual-phase steels. Scripta Metallurgica, 1987, 21, 1663-1667.	1.2	10
250	FORMING BEHAVIOUR OF TAILOR (LASER) WELDED BLANKS OF AUTOMOTIVE STEEL SHEET. Canadian Metallurgical Quarterly, 2006, 45, 189-198.	0.4	10
251	Fabrication and mechanical properties of silicon carbide–aluminum oxynitride nanocomposites. Ceramics International, 2014, 40, 14295-14303.	2.3	10
252	Tensile and Fatigue Properties of Single and Multiple Dissimilar Welded Joints of DP980 and HSLA. Journal of Materials Engineering and Performance, 2017, 26, 783-791.	1.2	10

#	Article	IF	CITATIONS
253	Fracture Characteristics and Analysis in Dissimilar Cu-Al Alloy Joints Formed via Electromagnetic Pulse Welding. Materials, 2019, 12, 3368.	1.3	10
254	Crack initiation and growth in a special quasi-sandwich crossed-lamellar structure in Cymbiola nobilis seashell. Journal of the Mechanical Behavior of Biomedical Materials, 2019, 90, 104-112.	1.5	10
255	Tensile and cyclic deformation response of friction-stir-welded dissimilar aluminum alloy joints: Strain localization effect. Journal of Materials Science and Technology, 2021, 73, 91-100.	5.6	10
256	A new geometric correction factor for a finite width center cracked plate loaded by two pairs of splitting forces. International Journal of Fracture, 1993, 61, R43-R50.	1.1	9
257	Interfacial reactions in Ti–Fe particles reinforced hydroxyapatite matrix composites. Materials Letters, 2014, 128, 245-247.	1.3	9
258	Achieving high damping capacity and strength simultaneously in a high-zinc aluminum alloy via melt spinning and hot extrusion. Materials Science & Engineering A: Structural Materials: Properties, Microstructure and Processing, 2022, 833, 142376.	2.6	9
259	Cyclic deformation behavior and fatigue life modeling of CNT-reinforced heterogeneous aluminum-based nanocomposite. Materials Science & Engineering A: Structural Materials: Properties, Microstructure and Processing, 2022, 840, 142881.	2.6	9
260	Cyclic deformation behavior and fatigue life prediction of an automotive cast aluminum alloy: A new method of determining intrinsic fatigue toughness. Fatigue and Fracture of Engineering Materials and Structures, 2022, 45, 725-738.	1.7	9
261	The relationship between superconductivity and microstructure through the fractal dimensions in Y-Ba-Cu-O compounds. Journal of Physics C: Solid State Physics, 1988, 21, L271-L276.	1.5	8
262	Numerical evaluation of stress distributions ahead of crack tip for finite-width center cracked specimens II. Loaded by a pair of tensile forces on the center line of specimen. International Journal of Fracture, 1994, 66, R57-R63.	1.1	8
263	Fabrication of Magnesium–NiTip Composites via Friction Stir Processing: Effect of Tool Profile. Metals, 2020, 10, 1425.	1.0	8
264	Fracture Toughness of High Melting Point Materials. High Temperature Materials and Processes, 1994, 13, 75-86.	0.6	7
265	Fractal characteristics of pitting under cyclic loading. Materials Letters, 1989, 7, 473-476.	1.3	6
266	Localized Cyclic Strain Measurements of Friction Stir Welded Aluminum Alloy Using a Flat-Clad Optical Fiber Sensor Array. IEEE Sensors Journal, 2010, 10, 888-892.	2.4	6
267	Residual Stresses and Tensile Properties of Friction Stir Welded AZ31B-H24 Magnesium Alloy in Lap Configuration. Metallurgical and Materials Transactions B: Process Metallurgy and Materials Processing Science, 2015, 46, 1626-1637.	1.0	6
268	Interaction between nano-precipitates and dislocations during high temperature deformation of Al-Si alloys. Journal of Alloys and Compounds, 2017, 712, 219-224.	2.8	6
269	Deformation and fracture behavior of a natural shell ceramic: Coupled effects of shell shape and microstructure. Materials Science and Engineering C, 2018, 90, 557-567.	3.8	6
270	Effects of Mo and B Additives on Hardness and the Resistance of Cu–Ni Alloy to Wear, Corrosion and Corrosive Wear. Metals and Materials International, 2021, 27, 4911-4921.	1.8	6

#	Article	IF	CITATIONS
271	Cyclic Deformation Behavior of A Heat-Treated Die-Cast Al-Mg-Si-Based Aluminum Alloy. Materials, 2020, 13, 4115.	1.3	6
272	Achieving Superior Superplasticity in a Mg–6Al–Zn Plate via Multi-pass Submerged Friction Stir Processing. Acta Metallurgica Sinica (English Letters), 2022, 35, 757-762.	1.5	6
273	Microstructural and mechanical aspects of laser metal deposited H13 powder for die repair. Materials Today Communications, 2021, 29, 102945.	0.9	6
274	Cyclic plasticity of recrystallized Mo at low temperatures. Materials Science & Engineering A: Structural Materials: Properties, Microstructure and Processing, 1997, 234-236, 766-769.	2.6	5
275	Effect of a hard artificial asperity on the crack closure behavior in an annealed SAE 1015 steel. Engineering Fracture Mechanics, 2005, 72, 2106-2127.	2.0	5
276	Microstructural Characterization and Fatigue Properties of 2195 Al-Li Alloy. Materials Science Forum, 2006, 519-521, 147-152.	0.3	5
277	Tensile Properties and Strain Hardening Behavior of a Friction Stir Welded AA2219 Al Alloy. Advanced Materials Research, 2011, 291-294, 833-840.	0.3	5
278	Pressure-induced phase transition of lead phosphate Pb ₃ (PO ₄) ₂ : X-ray diffraction and XANES. Phase Transitions, 2014, 87, 1255-1264.	0.6	5
279	Cyclic Deformation of Rare-Earth Containing Magnesium Alloys. Advanced Materials Research, 0, 891-892, 391-396.	0.3	5
280	Analysis of Microstructural Changes in the Heat-Affected Zone and Fusion Zone of a Fiber Laser Welded DP980 Steel. Metallurgical and Materials Transactions B: Process Metallurgy and Materials Processing Science, 2015, 46, 1638-1646.	1.0	5
281	Aging characteristics of the Al-Si-Cu-Mg cast alloy modified with transition metals Zr, V and Ti. IOP Conference Series: Materials Science and Engineering, 2016, 117, 012031.	0.3	5
282	Silicon Nitride Whisker-Reinforced Aluminum Matrix Composites: Twinning and Precipitation Behavior. Metals, 2020, 10, 420.	1.0	5
283	Hierarchical Morphology and Formation Mechanism of Collision Surface of Al/Steel Dissimilar Lap Joints via Electromagnetic Pulse Welding. Metals, 2021, 11, 1468.	1.0	5
284	Active Slip Mode Analysis of an Additively Manufactured Ti-6Al-4V Alloy via In-Grain Misorientation Axis Distribution. Metals, 2022, 12, 532.	1.0	5
285	Microplastic Relaxations of Single and Polycrystalline Molybdenum. Physica Status Solidi A, 1998, 167, 43-60.	1.7	4
286	Effect of boron and carbon on thermomechanical fatigue of IN 718 superalloy. Materials Science & Engineering A: Structural Materials: Properties, Microstructure and Processing, 2006, 437, 172-182.	2.6	4
287	Monotonic and Fatigue Behavior of Magnesium Extrusion Alloy AM30: An International Benchmark Test in the "Magnesium Front End Research and Development Project― , 2010, , .		4
288	Ultrasonic Spot Welding of an Aluminum Alloy for Automotive Applications. Materials Science Forum, 0, 941, 735-740.	0.3	4

#	Article	IF	CITATIONS
289	Influence of process parameters on the sintering behaviour and densification of NiAl intermetallics fabricated by spark plasma sintering. Materials Today: Proceedings, 2021, 38, 1159-1163.	0.9	4
290	Cyclic hardening behavior and deformation mechanisms of friction-stir-welded dissimilar AA5083-to-AA2024 joints with heterogeneous microstructures. Materials Characterization, 2021, 181, 111465.	1.9	4
291	Microstructural Evaluation of Friction Stir Processed AZ31B-H24 Magnesium Alloy. Canadian Metallurgical Quarterly, 2007, 46, 425-432.	0.4	4
292	Microstructure and Electrochemical Behavior of a 3D-Printed Ti-6Al-4V Alloy. Materials, 2022, 15, 4473.	1.3	4
293	Lattice distortions due to oxygen migration in the Y-Ba-Cu-O system. Physics Letters, Section A: General, Atomic and Solid State Physics, 1987, 126, 58-60.	0.9	3
294	Laserinterferometer zur berührungslosen Messung von Lägenäderungen im Nanometer-Bereich. Materialwissenschaft Und Werkstofftechnik, 1992, 23, 197-200.	0.5	3
295	Experimental K-calibration of elliptical surface cracks under bending. Engineering Fracture Mechanics, 1993, 44, 437-448.	2.0	3
296	Geometric correction factors determined by force balance method for center cracked specimens. VI. Loaded by a pair of splitting forces acting at an arbitrary location on the crack. International Journal of Fracture, 1993, 64, R89-R96.	1.1	3
297	Geometric correction factors determined by force balance method for center cracked specimens. IX Loaded by a portion of unsymmetric stresses on the crack. International Journal of Fracture, 1995, 73, R47-R58.	1.1	3
298	Numerical evaluation of stress distributions ahead of crack tip for finite-width center cracked specimens. International Journal of Fracture, 1996, 75, R3-R8.	1.1	3
299	Formation of metal nanoparticles in silica by the sequential implantation of Ag and Cu. Applied Physics A: Materials Science and Processing, 2007, 89, 681-684.	1.1	3
300	Characterization of Isothermally Heat-Treated High Carbon Nanobainitic Steels. Journal of Materials Engineering and Performance, 2013, 22, 3070-3076.	1.2	3
301	Hydroxyapatite reinforced with Ti–Fe particle: correlation between composition, microstructure and mechanical properties. Advances in Applied Ceramics, 2014, 113, 108-113.	0.6	3
302	Introducing a New Member of the Editorial Board of Metallography, Microstructure, and Analysis. Metallography, Microstructure, and Analysis, 2016, 5, 1-1.	0.5	3
303	Microstructure and Texture Evolution in a Yttrium-Containing ZM31 Alloy: Effect of Pre- and Post-deformation Annealing. Metallurgical and Materials Transactions B: Process Metallurgy and Materials Processing Science, 2016, 47, 3318-3325.	1.0	3
304	Crystallographic texture of crossed-lamellar structure in <i>Cymbiola nobilis</i> shell. Journal of the Ceramic Society of Japan, 2017, 125, 419-422.	0.5	3
305	Ultrasonic spot welding of dissimilar 2024Al alloy and SiCp/2009Al composite. Proceedings of the Institution of Mechanical Engineers, Part L: Journal of Materials: Design and Applications, 2018, , 146442071880913.	0.7	3
306	Reducing Yield Asymmetry between Tension and Compression by Fabricating ZK60/WE43 Bimetal Composites. Materials, 2020, 13, 249.	1.3	3

#	Article	IF	CITATIONS
307	Stretch Formability of an AZ61 Alloy Plate Prepared by Multi-Pass Friction Stir Processing. Materials, 2021, 14, 3168.	1.3	3
308	Effect of Boron Concentration on Fatigue Crack Propagation Resistance and Low Cycle Fatigue Properties of INCONEL 718. , 2004, , .		3
309	Geometric correction factors determined by force balance method for center cracked specimens V. Loaded by a pair of tensile forces acting at some distance from the crack. International Journal of Fracture, 1993, 62, R71-R79.	1.1	3
310	An artful microstructure in nacre: Superior resistance to fatigue deformation. International Journal of Fatigue, 2022, 157, 106705.	2.8	3
311	A new model of the fatigue crack growth threshold. Philosophical Magazine Letters, 1989, 59, 309-316.	0.5	2
312	Experimental calibration for surface flaws under bending for different materials and stress ratios. Engineering Fracture Mechanics, 1994, 49, 473-485.	2.0	2
313	Experimental K-calibration for corner cracks under bending loading. International Journal of Fatigue, 1995, 17, 545-550.	2.8	2
314	Title is missing!. Journal of Materials Science Letters, 1998, 17, 865-867.	0.5	2
315	Geometric correction factors for center cracked specimens subjected to nonlinear bridging stresses in the shear lag model. Engineering Fracture Mechanics, 2003, 70, 823-829.	2.0	2
316	Derivation of applied stress-crack opening displacement relationships for the evaluation of effective stress intensity factor range. International Journal of Fracture, 2004, 125, 371-386.	1.1	2
317	Application of Flat-Clad Optical Fiber Bragg Grating Sensor in Characterization of Asymmetric Fatigue Deformation of Extruded Magnesium Alloy. IEEE Sensors Journal, 2011, 11, 3042-3046.	2.4	2
318	Effect of Iron on the Sinterability and Properties of HA/Ti-Fe Composites. Advanced Materials Research, 2014, 898, 271-274.	0.3	2
319	Recrystallization mechanisms during high-temperature XRD and oxidation behavior of CNT-reinforced NiAl composites. Corrosion Science, 2022, 204, 110384.	3.0	2
320	Geometric correction factors determined by force balance method for center cracked specimens. VII. Loaded by uniformly distributed stresses acting on central portion of crack. International Journal of Fracture, 1994, 68, R9-R14.	1.1	1
321	Geometric correction factors determined by force balance method for center cracked specimens VIII. Loaded by two parts of uniformly distributed stresses acting on the crack. International Journal of Fracture, 1995, 70, R35-R44.	1.1	1
322	Numerical evaluation of stress distributions ahead of crack tip for finite-width center cracked specimens. IV. Loaded by a pair of splitting forces acting at an arbitrary location on the crack. International Journal of Fracture, 1996, 76, R3-R9.	1.1	1
323	Cyclic deformation of extruded AM30 magnesium alloy in the transverse direction. Journal of Physics: Conference Series, 2010, 240, 012048.	0.3	1
324	Microstructure in Pressureless-Sintered Iron-Containing Hydroxyapatite/Titanium Composites. Advanced Materials Research, 2010, 160-162, 1582-1587.	0.3	1

#	Article	IF	CITATIONS
325	Reply to comments on "An improved model for bainite formation at isothermal temperatures― Scripta Materialia, 2011, 65, 373-375.	2.6	1
326	Effect of Fiber Laser Welding on the Fatigue Properties of Dissimilar Welded Joints between DP980 and HSLA Steels. , 0, , .		1
327	Effect of Strain Level on the Behavior of Intermetallics and Texture of Al-Si-Cu-Mg Alloy Modified with Transition Metals. SAE International Journal of Materials and Manufacturing, 2015, 8, 731-735.	0.3	1
328	Effect of Transition Metals on Thermal Stability of Al‒Si Cast Alloys. , 2018, , 287-296.		1
329	Effect of Auto-Tuning on Serrated Flow Behavior. Metals, 2019, 9, 845.	1.0	1
330	A New Mechanism of Dynamic Phase Transformations in An Isothermal Forged Beta–Gamma Intermetallic Alloy. Materials, 2019, 12, 2787.	1.3	1
331	In Situ AFM Analysis of Surface Electron Behaviors of Strainâ€Free and Deformed Ferrite and Austenite in Duplex Steel and Their Correlation with Electron Work Function. Physica Status Solidi (A) Applications and Materials Science, 2019, 216, 1800933.	0.8	1
332	Similar and Dissimilar Ultrasonic Spot Welding of a Rare-Earth Containing ZEK100 Magnesium Alloy. , 2016, , 109-113.		1
333	Resistance Spot Welding Characteristics and Mechanical Properties of Galvannealed HSLA 350 Steel. Canadian Metallurgical Quarterly, 2009, 48, 303-310.	0.4	1
334	Texture Development in an Extruded Magnesium Alloy During Compression Along the Transverse Direction. , 2013, , 313-316.		1
335	Effect of Microstructure Evolution on Corrosion Behavior of Friction Stir Welded Joint for 2195-T8 Alloy. Corrosion, 2020, 76, .	0.5	1
336	Effect of polarizable atmospheres on superconductivity of the Y-Ba-Cu-O compounds. Applied Physics A: Solids and Surfaces, 1989, 48, 355-357.	1.4	0
337	Geometric correction factors determined by force balance method for center cracked specimens. X International Journal of Fracture, 1996, 78, R3-R8.	1.1	Ο
338	Numerical evaluation of stress distributions ahead of crack tip for finite-width center cracked specimens. V International Journal of Fracture, 1996, 79, R45-R50.	1.1	0
339	Geometric correction factors determined by force balance method for center cracked specimens. International Journal of Fracture, 1996, 81, R63-R69.	1.1	Ο
340	Influence of Weld Simulation on the Microstructure and Fatigue Strength of 2195 Aluminum-Lithium Alloy. Materials Science Forum, 2000, 331-337, 1769-1774.	0.3	0
341	Influence of Heat Treatment on Fatigue Resistance of Electron Beam Welded Dissimilar Titanium Alloy Joints. Advanced Materials Research, 0, 891-892, 1539-1544.	0.3	0
342	Static recrystallization of pure titanium after cryo-deformation. Journal of Physics: Conference Series, 2019, 1270, 012040.	0.3	0

#	Article	IF	CITATIONS
343	Fatigue and Deformation of Light Magnesium Alloys. Structural Integrity, 2019, , 126-132.	0.8	0
344	Nonlinearity of Material Loss Versus the Wearing Force. Jom, 2019, 71, 4274-4283.	0.9	0
345	Fiber laser welding of hot stamping steel: effect of in situ annealing on the microstructure and mechanical properties. Welding in the World, Le Soudage Dans Le Monde, 2021, 65, 57-65.	1.3	0
346	Monotonic and Fatigue Behavior of Mg Alloy Friction Stir Spot Welds: An International Benchmark Test in the "Magnesium Front End Research and Development―Project. , 2011, , 629-634.		0
347	Effect of Yttrium Addition on Texture Development in a Cast Mg-Al-Y Magnesium Alloy During Compression. , 2014, , 269-272.		0
348	Low Cycle Fatigue of Aluminum-Silicon Alloys for Power-Train Applications. , 2015, , 999-1006.		0
349	Hot Deformation and Processing Map in an Mg-Zn-Mn-Y Alloy. , 2016, , 183-186.		0
350	Tensile Behavior of a Titanium Alloy Additively Manufactured via Selective Electron Beam Melting. Structural Integrity, 2020, , 14-19.	0.8	0
351	A Simple Surface Treatment for Mg to Gain Enhanced Resistance to Corrosion and Corrosive Wear by Hammering Al Powderâ€Covered Mg Substrate. Advanced Materials Interfaces, 0, , 2200087.	1.9	Ο